ARTICLES
PUBLISHED ONLINE: 23 MARCH 2014 | DOI: 10.1038/NMAT3915
nature materials

Strong, tough and stiff bioinspired ceramics from brittle constituents

Florian Bouville[1,2], Eric Maire[2], Sylvain Meille[2], Bertrand Van de Moortèle[3], Adam J. Stevenson[1] and Sylvain Deville[1]*

High strength and high toughness are usually mutually exclusive in engineering materials. In ceramics, improving toughness usually relies on the introduction of a metallic or polymeric ductile phase, but this decreases the material's strength and stiffness as well as its high-temperature stability. Although natural materials that are both strong and tough rely on a combination of mechanisms operating at different length scales, the relevant structures have been extremely difficult to replicate. Here, we report a bioinspired approach based on widespread ceramic processing techniques for the fabrication of bulk ceramics without a ductile phase and with a unique combination of high strength (470 MPa), high toughness (17.3 MPa $m^{1/2}$), and high stiffness (290 GPa). Because only mineral constituents are needed, these ceramics retain their mechanical properties at high temperatures (600 °C). Our bioinspired, material-independent approach should find uses in the design and processing of materials for structural, transportation and energy-related applications.

Ceramics exhibit among the highest stiffness and strength of all known material classes[1]. Because of the strong and directional bonding between constitutive atoms, they present a high fusion temperature and thus a high thermal stability. Being composed of mostly light elements, they are also lightweight compared to most metals. This property combination predestined them to be the best material choice for high-stress and high-temperature operating conditions. However, the iono-covalent bonds limit most common plasticity mechanisms and therefore prevent any ductile behaviour. This lack of plasticity is often the main limitation for the use of ceramic materials, resulting frequently in catastrophic and unpredictable failure[2], which greatly limits their range of applications. Damage-resistant ceramics are thus in great demand.

However, countless damage-resistant biological materials comprise ceramics and are used for structural purposes[3,4] in nature. The most famous example is probably the nacreous part of seashells, where a brick-and-mortar structure comprised of 95 vol.% of platelets of polycrystalline aragonite ($CaCO_3$) and 5 vol.% of a protein is extremely effective at restricting crack propagation[5] and presents a toughness orders of magnitude greater than either of its constituents[6,7]. Nacre toughness is achieved through numerous extrinsic mechanisms that include viscoelastic deformation of the protein layer[8], mineral bridge rupture, and inelastic shearing and frictional sliding during platelet pull out[5].

Tough ceramic materials could be obtained by translating the specific microstructural and interfacial structures present in natural systems to engineering materials[9]. This could be achieved by building brick-and-mortar organized structures using anisotropic particles as building blocks combined with a ductile phase. The alignment of anisotropic particles can be achieved by sequential deposition methods[10] for thin films but not for bulk materials.

Ceramic/polymer composites that replicate nacre features have been fabricated by various techniques, such as ice templating, magnetic particle alignment[9], or simply by gluing ceramic layers[11], and the toughness levels achieved are rather impressive[12]. Processes using magnetic fields lead to structures with well-aligned platelets embedded in a polyurethane matrix[13]. Such approaches nevertheless suffer from severe limitations. Because the design is based on the presence of a ductile phase, the materials exhibiting the highest toughness all comprise at least 20 vol.% of a polymeric phase, restricting de facto their useful temperature range to mild temperatures (200 °C or less). In nacre and nacre-inspired materials, the intrinsic toughening is primarily a result of crack deflection at the platelet interfaces. Thus, as a first-order approximation, increasing the local density of interfaces should increase the toughness of the material. Such an increase can be achieved by the use of small constituents. Finally, the processing route still includes too many steps to make it viable beyond the lab scale.

Here we demonstrate the use of a relatively simple processing route based on widespread ceramic processing techniques to obtain fully ceramic, layered bulk materials with submicrometre layer spacings that exhibit not only an unprecedented toughness for a ceramic material but also, because it comprises only mineral constituents, a very high strength and stiffness even at high temperature.

Processing strategy

Inspired by structural guidelines derived from the study of nacre, we fabricated (see Methods and Supplementary Information) dense ceramic materials defined by five structural features, spanning several length scales (Fig. 1a): long-range structural order; closely packed ceramic platelets of dimensions identical to that of nacre; ceramic bonds (bridges) linking the platelets; nano-asperities at the surface of platelets; and a secondary phase with lower stiffness ensuring load redistribution, crack deflection, and delamination.

The process we used here is based on ice-templating. However, we did not rely on ice crystals to form the elementary bricks, but instead took advantage of their growth as a driving force for

[1]Laboratoire de Synthèse et Fonctionnalisation des Céramiques, UMR3080 CNRS/Saint-Gobain, Cavaillon F-69621, France. [2]Université de Lyon, INSA-Lyon, MATEIS CNRS UMR5510, Villeurbanne 84306, France. [3]Laboratoire de Géologie de Lyon, Ecole Normale Supérieure de Lyon, Lyon 69364, France. *e-mail: sylvain.deville@saint-gobain.com

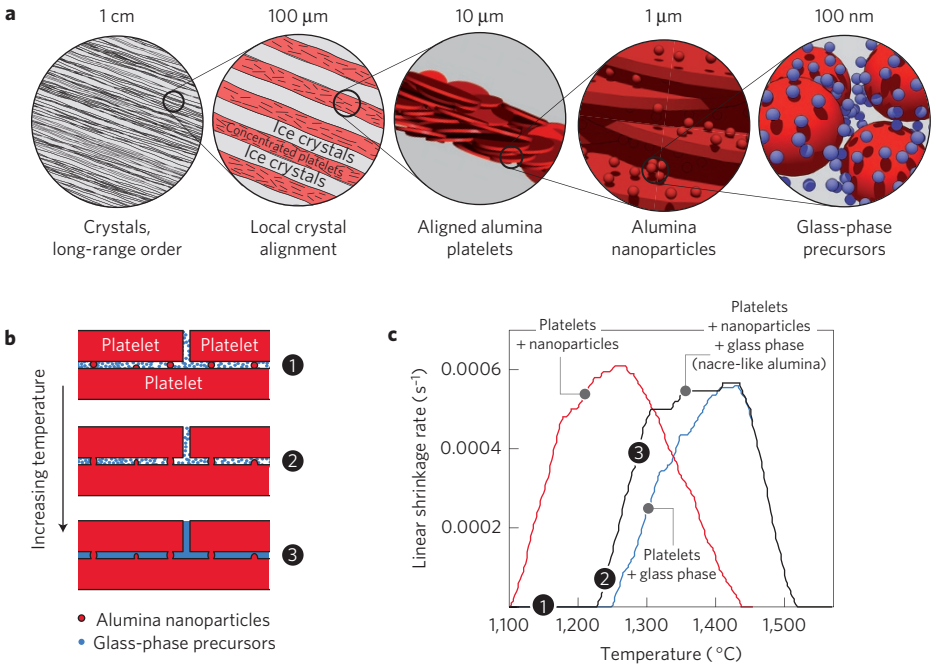

Figure 1 | Design strategy describing the control at multiple scales of structural self-organization, and densification strategy. **a**, Self-organization of all the structural features occurs during the freezing stage. The growth of ordered-ice crystals triggers the local alignment of platelets. Alumina nanoparticles and liquid-phase precursors are entrapped between the platelets. **b**, Schematic representation of the densification scenario. **c**, The linear shrinkage rate illustrates that the densification of the composition comprising either one of the building blocks (3 vol.% nanoparticles or 5 vol.% liquid phase) occurs at different temperatures. In the composition comprising all the building blocks, the densification starts at a temperature between the two other compositions (liquid phase only and nanoparticles only), showing an interaction between nanoparticles and liquid-phase precursors.

the local self-assembly of anisotropic particles (platelets, Fig. 1a). Those particles have the same dimensions as nacre platelets (500 nm thickness, 7 µm diameter), and constitute the elementary building blocks of the structure. When a suspension is directionally frozen, the metastable growth of the ice crystals[14] repels and concentrates the particles present in the suspension. The concentration of the particles occurs at a length scale where self-assembly of platelets can occur[15] (Fig. 1a). Alumina nanoparticles (100 nm) incorporated in the initial suspension serve as a source of both inorganic bridges between the platelets and nanoasperities at the surface of platelets, similar to that observed in nacre. Finally, smaller nanoparticles (20 nm) of liquid-phase precursors (silica and calcia) are added to aid filling the remaining gaps during the sintering stage. The material is thus composed of 98.5 vol.% alumina, 1.3 vol.% of silica, and 0.2 vol.% of calcia. This simple strategy, where all the constituents are incorporated in the initial suspension and self-organized in one step, allows precise and easy tailoring of the final material composition. Long-range order of the ice crystals is obtained through a freezing under a flow method (Supplementary Methods). Once the porous samples are obtained, they are simply pressed and sintered by field assisted sintering (FAST). The materials are 86% porous after the freeze drying step. The pressing step (100 MPa) prior to sintering is critical to remove almost all of the macroporosity. This is easily achieved thanks to the long-range order of the macropores induced by the controlled freezing step.

Due to their size and high aspect ratio, the platelets themselves are unlikely to densify by sintering. Instead, formation of a liquid phase rearranges the particles through capillary forces, facilitating platelet packing under the applied load by lubricating the contact points and by filling the pore space between them (Fig. 1b). At the same time, the nanometric alumina particles form strong bridges by sintering to the platelets. The high surface area and surface curvature of nanoparticles allow them to sinter at lower temperatures than the platelets[16] (Fig. 1c). One important consideration is ensuring that the alumina nanoparticles are not completely dissolved in the liquid phase by either limiting the total amount of liquid phase, or by using short processing times such as those employed here (enabled by the rapid, pressure-assisted densification method). The sample with liquid phase starts shrinking at a higher temperature (Fig. 1c) than the sample without the liquid phase. We selected this glass composition (calcia and silica) for its very high melting temperature (pure silica starts melting at around 1,600 °C). We believe that the precursor particles of the glass phase prevent most of the contacts between alumina platelets and the nanoparticles, and thus delay the densification of the alumina nanoparticles. The glass has to melt first before densification can proceed. In addition, because the liquid-phase precursors are well dispersed in the system and in low concentration compared to the alumina platelets and nanoparticles, the local composition throughout the green body is not likely to be the liquid-phase composition predicted from the phase diagram—there must be some diffusion and densification before the liquid phase formation. Along with the physical restraint described above, this may contribute to the slower densification kinetics observed.

The entire process thus consists of three steps: preparation of an aqueous colloidal suspension containing all the required building blocks and processing additives, ice templation of this suspension, and a pressure-assisted sintering step at 1,500 °C. The materials obtained are referred to as nacre-like alumina.

Comparison of microstructures

The final microstructure of nacre-like alumina (Fig. 2) is characterized by a dense packing of platelets presenting long-range order. The use of a fast sintering method limits grain growth so that the initial dimensions of the platelets are retained. A bulk material with submicron layer spacing is thus obtained, a feature of nacre that had proved impossible to replicate so far in bulk materials. Compared to the microstructure of nacre (Fig. 2a,b), the

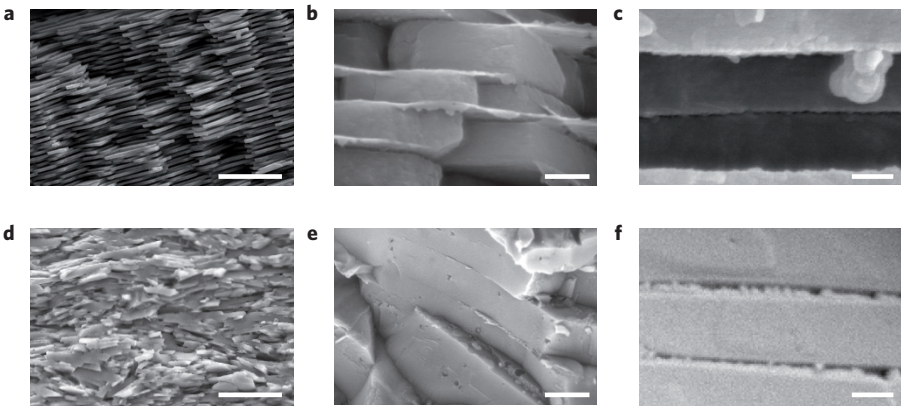

Figure 2 | Comparison of microstructures. Panels (**a**–**c**) correspond to nacre; panels (**d**–**f**) to nacre-like alumina. **a**,**d**, SEM micrographs showing the short- and long-range order of platelets. The nacre-like alumina shows relatively high organization of the platelets. **b**,**e**, Local stacking of platelets. A liquid-phase film is present even when the platelets are close, mimicking the protein layer in the nacre structure. **c**,**f**, Closer views of the platelet interface, revealing the presence of the inorganic bridges and nano-asperities along with the glassy (**f**), or organic (**c**), phase filling the space between adjacent platelets. Some residual pores are also visible. Scale bars, 10 μm (**a**,**d**); 500 nm (**b**,**e**); 250 nm (**c**,**f**).

packing of platelets presents short-range order (Fig. 2e), but the long-range order is not as perfect. The waviness of the stacking (Fig. 2d) in our nacre-like ceramic, estimated at ±15° around the main orientation, comes from the organization of the ice crystals. The long-range order is nevertheless sufficient to obtain nearly fully dense samples (for example, >98% of relative density). The relative densities calculated by the Archimedean method are very similar: platelets and nanoparticles: 98.9%, platelets and liquid phase: 98.4%, and platelets, nanoparticles and liquid phase: 98.8%.

Observations of the interfaces between platelets (Fig. 2e,f) reveal the presence of a secondary phase mimicking the organic layer in nacre (Fig. 2b). It also reveals some alumina bridges between adjacent platelets and, finally, nanoasperities analogous to those in nacre (Fig. 2c). Based on the experimental conditions and the ceramic phases present, this secondary phase is most probably amorphous. A small fraction of the alumina platelets and nanoparticles is dissolved into this glass phase at the interface, so that the actual final fraction of this phase (estimated to be around 2–3 vol.%) is slightly higher than that initially incorporated into the suspension (1.5 vol.%). We estimated the fraction of the glass phase based on the amount of glass precursors (initially 1.5 vol.%) and nanoparticles incorporated (initially 3 vol.%), and the corresponding ternary phase diagram (alumina–silica–calcia). Based on this phase diagram[17], we can estimate the composition of the glass phase at 10 wt.% SiO_2, 65 wt.% CaO and 25 wt.% Al_2O_3, although it is hard to tell whether equilibrium is achieved during the rapid densification.

The microstructure of the synthetic material is thus strikingly similar to that of natural nacre at several length scales, validating the possibility to fabricate bulk, centimetre-sized samples with only a few simple processing steps.

Ductile ceramics?

Single-edge notched beam (SENB) tests were carried out to measure the toughness, and the behaviour of the materials tested was compared with a reference polycrystalline alumina sample. The resulting stress–strain curves are plotted in Fig. 3a for three model compositions to illustrate the synergistic effects between the structural features introduced: platelets with nano-asperities, platelets with a liquid phase, and platelets with both (the nacre-like alumina structure). As expected, the samples containing the liquid phase only at the platelet interface exhibit a purely linear elastic response until a catastrophic failure occurs, with unstable crack propagation characteristic of brittle materials. The corresponding fracture surface, showing no crack deflection at all, is shown in Fig. 3d. The fracture toughness K_{Ic} (6.1 MPa $m^{1/2}$) is nevertheless already significantly higher than a reference alumina (3.5 MPa $m^{1/2}$), since platelets are significantly harder to separate than isotropic particles due to their orientations[18]. Platelets with nano-asperities exhibit a very significant toughening stage. Progressive failure occurs by stable crack propagation, a very unusual behaviour in pure ceramic materials.

When both reinforcements are combined, leading to the nacre-like alumina structure, we obtain stable crack growth combined with toughening, similar to that of nacre (reported for comparison in Fig. 3b). The nacre-like alumina, free of any ductile component, is clearly stiffer, with a flexural modulus of 290 GPa (compared to 40 GPa for nacre). The mechanical response, where more than 50% of the strain to failure is inelastic, is strikingly reminiscent of that observed in ductile metallic or organic materials, a remarkable and unexpected behaviour for a material exclusively composed of ceramic constituents. The reinforcement mechanisms (discussed in the section 'Toughening mechanisms') are extrinsic, which means that of course no true ductility (plastic deformation without crack propagation) is observed.

The fracture toughness, K_{Ic}, describes only the resistance to a crack initiation and is significantly higher in this nacre-like structure (6.2 MPa $m^{1/2}$) than in usual polycrystalline alumina (3.5 MPa $m^{1/2}$). It is nevertheless unable to describe the multiple extrinsic toughening mechanisms that take place during crack propagation and that greatly contribute to the dissipation of energy. The crack is deflected by the composite low-stiffness interface[19] (Fig. 3e) and slowed down by various extrinsic toughening mechanisms which result in stable crack growth, similar to natural nacre[5]. This toughening leads to an increase of the fracture resistance as the crack propagates. This behaviour, known as an R-curve effect, is characteristic of many natural materials such as nacre[5], bone[3,4], and tooth[20]. To measure the R-curve, the indirect crack length is measured by a compliance method (Methods). Crack extension reported here satisfied a small-scale bridging conditions (Methods). Analogous approaches have been used previously in similar structures[2,3,12], where multiple extrinsic toughening mechanisms needed to be described. The R-curves at room temperature and high temperature (600 °C) are plotted in Fig. 3c. According to the ASTM criterion, the maximum increase of toughness is extremely high, around 17.3 MPa $m^{1/2}$. This corresponds to a 300% increase compared to the K_{Ic} toughness (500% increase with respect to the reference alumina). This far exceeds that of nacre

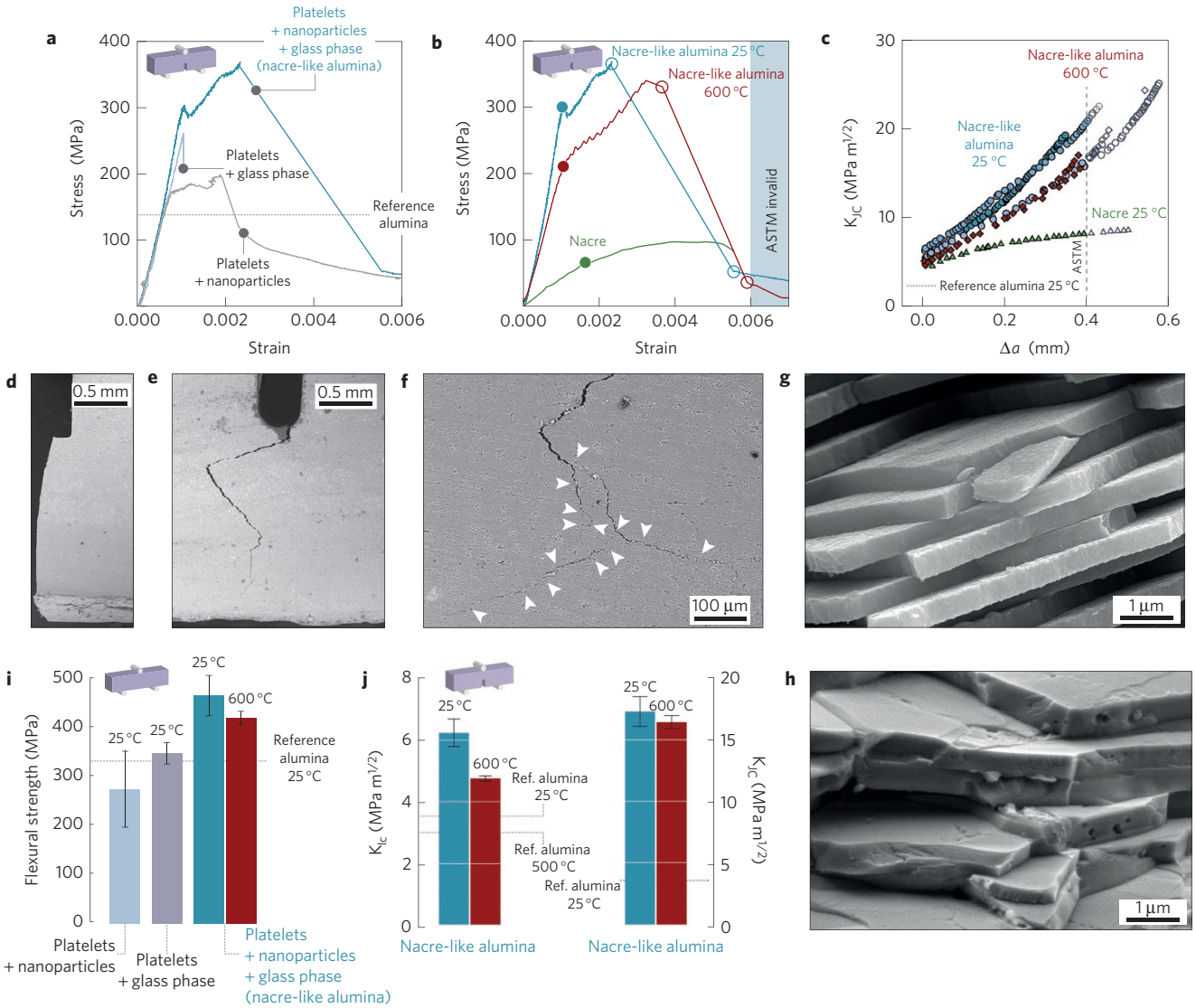

Figure 3 | Mechanical properties of nacre-like alumina and nacre. **a**, Stress–strain curve of the same three compositions on SENB samples. The 5 vol.% liquid phase presents brittle behaviour, the 3 vol.% nanoparticles phase presents toughening, and the combination leads to significant toughening. **b**, Stress–strain curve for SENB samples of nacre-like ceramic and natural nacre. The dots on the curve indicate the initiation of stable crack propagation. The circles indicate the beginning and end of unstable crack propagation. **c**, Fracture toughness calculated from the J-integral and crack extension Δa, and the equivalent for nacre-like alumina and nacre. **d**, Smooth fracture surface of brittle composition (platelets and liquid phase). **e**, Fracture surface of a nacre-like sample that shows long-range crack deflection. **f**, Multiple cracking and crack bridging towards the end of the crack path. Arrows indicate the onset of crack branching and bridging. **g**,**h**, Detail of the fracture surface in nacre (**g**) and nacre-like alumina (**h**), showing the crack deflection and delamination at the platelet interface. **i**, Flexural strength of three different compositions, liquid phase (5 vol.%) and platelets, nanoparticles (3 vol.%) and platelets, and nacre-like alumina (1.5 vol.% and 3 vol.% of liquid phase and nanoparticles, respectively). The dotted line corresponds to an equiaxed fine-grain alumina in **a** and **i**. Error bars indicate standard deviation. **j**, Comparison of toughness for crack initiation (K_{Ic}) and stable crack propagation (K_{JC}) in nacre-like alumina and reference alumina at room temperature (25 °C) and high temperature[39] (600 °C).

and is equivalent to the best brick-and-mortar polymer/ceramic composites developed previously[12].

The second stage of crack growth, when the crack length exceeds 400 µm, is unstable. Nevertheless, different energy-dissipating mechanisms are present, eventually leading to the arrest of cracks before catastrophic failure can occur (Fig. 3e,f). Notch-free samples are not fully broken after being exposed to their maximum stresses, which provides further evidence of the efficiency of the reinforcement in these materials.

The properties are retained at relatively high temperature (600 °C, Fig. 3b), with a stress intensity factor for crack initiation (K_{Ic}) of 4.7 MPa m$^{1/2}$ and a maximum toughness K_{JC} of 16.4 MPa m$^{1/2}$ (Fig. 3j).

Toughening mechanisms

We combine with these materials a number of toughening mechanisms, operating at different length scales. By restricting our choice of constituents to ceramic materials so as to ensure their use at high temperature and maximize the stiffness, we are also eliminating most of the usual toughening mechanisms seen in ductile materials, such as dislocation plasticity or shear bands. The extrinsic reinforcement developed here is derived from the hierarchical architecture of the material and the load redistribution resulting from the brick-and-mortar architecture. Crack deflection (Fig. 3e), multiple cracking, crack bridging and crack branching (Fig. 3f), and delamination (Fig. 3h), operate at the crack tip, effectively relieving the locally high stresses. The alumina

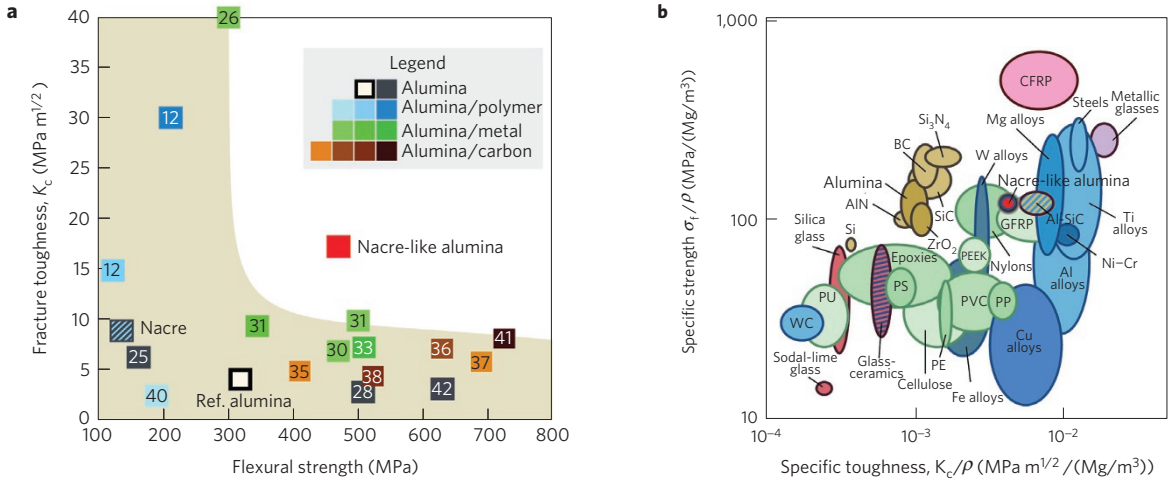

Figure 4 | Comparison of the relative materials performance. **a**, The conflict between strength and toughness: fracture toughness versus flexural strength for alumina-based materials. Improvements in toughness are obtained by the introduction of a ductile phase, such as a metallic phase[23,27–31], a polymer[12,40], or carbon reinforcements such as graphene[35], carbon nanotubes[32–34], or whiskers[41]. Improvements in strength are achieved through a texturation of the grains[25], hot isostatic pressing[42] or the addition of strong reinforcements. **b**, Ashby diagram of specific strength versus specific toughness for a range of engineering and natural materials[43]. The nacre-like aluminas have specific strength/toughness properties similar to those of GFRP. CFRP, carbon-fibre-reinforced polymers; GFRP, glass-fibre-reinforced polymers; PEEK, polyether ether ketone.

nanoparticles provide both bridges between the platelets and nano-asperities. This leads to efficient energy dissipation by frictional sliding during platelet pull-out and breaking of the bridges. Pores located between adjacent platelets, as seen in Fig. 2f, may also contribute by acting as local crack arresters by a Cook–Gordon mechanism[21]. The possibility to achieve toughness through a proper combination of brittle constituents has been recently hypothesized[22]. With the proper topological arrangement and stiffness ratio between two brittle phases, the stress concentration around the crack tip can be reduced thanks to a more efficient load redistribution. The deformation is delocalized, and strain redistributes throughout the entire structure. These mechanisms are likely to contribute to the level of toughness achieved in these structures. Further work will be necessary to quantify the relative contributions of all the toughening mechanisms identified here.

A high-strength, high-toughness material

The flexural strengths of our materials are reported in Fig. 3i. Platelets combined with either the liquid phase or the nano-asperities alone have, as expected, a flexural strength equivalent to or lower than the reference alumina. The nacre-like alumina exhibits a flexural strength of 470 MPa at room temperature and 420 MPa at 600 °C, a value essentially similar to that of the reference alumina. The presence of pores (defects) in the platelets and nanoparticle material may explain its lower strength. The synergistic combination of both the liquid phase and the nano-asperities is thus strikingly demonstrated by these measurements. The strength is similar in the transverse direction (490 MPa perpendicular to the basal plane of the platelets). This material does not present strength anisotropy, and thus any weakness, in these two solicitation directions. Because of sample size limitations (maximum thickness around 5 mm), the strength in the delamination direction cannot be assessed.

Strength and toughness are generally considered to be mutually exclusive[2]. Because intrinsic toughening mechanisms are linked to plasticity and thus strength, a compromise is always reached in structural materials where either one of the properties is set aside. In similar work[12], for instance, the introduction of 20 vol.% of a polymeric phase to increase the toughness resulted in a notable decrease of the flexural strength. Further toughness increases can be achieved through the addition of up to 60 vol.% Al–Si alloy[23], but no appreciable gains in strength are obtained. The introduction of a polymer or a metallic phase is thus always done at the expense of strength, stiffness, and temperature range of use. The toughness of the nacre-like alumina is greater than that of other reported values for alumina[24], textured alumina[25], or even for alumina composites[26], composed of either an organic phase[12], a metallic phase[27–31], or carbon reinforcements such as carbon nanotubes[32–34] or graphene[35] (Fig. 4a). As in nacre, the organization of the microstructure induces the emergence of improved properties without compromise, even at elevated temperature.

When it comes to materials choice, in particular for structural applications, the density is a major consideration. Metallic glasses are some of the toughest engineered materials produced so far, but their high density limits their use. Thickness is also a major problem because the necessary cooling rates cannot always be achieved on bulk samples. The unique combination of specific strength (σ_f/ρ) and specific toughness (K_c/ρ) of our bioinspired ceramic material actually matches that of glass-fibre-reinforced plastics (GFRP; Fig. 4b) while exhibiting higher hardness (16 GPa), stiffness and operating temperature. Because only ceramic constituents are used, the stiffness, strength and operating temperature of our material are at the usual level of engineering technical ceramics, highlighting their remarkable potential in structural and energy-related applications.

For now, the dimensions of the samples are limited to a few centimetres in diameter and a few millimetres in thickness. Two steps of the process induce size constraints: freezing and sintering. Although ice-templating has been restricted to the laboratory scale so far, there are no fundamental reasons why the process could not be scaled up. Large-scale, low-temperature processes are widespread in the industry (frozen food being the most notable example). The sintering process is actually very similar to hot pressing, except that an electric field is used to heat rapidly the graphite die. This kind of pressure-assisted equipment, assisted by an electric field, is now routinely used and widespread, and pieces up to 80 cm diameter are routinely sintered for a wide range of applications. With a few exceptions such as refractory materials for furnaces, which can have a thickness of half a metre or so, technical-ceramics pieces are almost always within this range of dimensions or even

smaller. The majority of technical ceramics pieces have dimensions in the millimetre range. We therefore believe that this approach should fulfil the requirements for most structural applications of ceramics, such as molten metal processing and forming or high-performance engines.

In the longer term, we believe that the design principles shown here are not restricted to ice templating, but could be adapted to standard colloidal processing routes for specific shapes, sizes, or directionality. We are currently investigating such ideas. The main issue we can expect, if standard colloidal processing routes are to be used, is how to control the orientation of anisotropic particles.

Concluding remarks

The bioinspired, material-independent design presented here is a specific but relevant example of a strong, tough, and stiff material, in great need for structural, transportation, and energy-related applications where catastrophic failure is not an option. The flexibility in the choice of materials permits an independent assessment (and thus tailoring) of the role of each structural feature on the mechanical properties, which is not possible in natural materials. Beyond structural materials, we expect to see many other benefits of using ice crystals as a driving force for the bulk self-organization of elementary building blocks. We are now focused on extending the concepts demonstrated here to other material combinations.

Methods

Suspensions preparation. A system composed of alumina platelets (7 μm diameter, 500 nm thickness), alumina nanoparticles (diameter around 100 nm), and a silica–calcia liquid phase (diameter around 20 nm) have been used. All the constituents where added in distilled water and then ball-milled for 24 h, except the alumina platelets that have been added 3 h before the end of the cycle to avoid any excessive breakage by the milling media.

Freezing under flow. To obtain dense structures by pressing the porous sample obtained after ice templating, further control of the crystal growth is needed to obtain parallel crystals over large dimensions. We use a method in which we let the slurry flow on the cooling plate where freezing occurs, leading to a second perpendicular temperature gradient during the freezing. A 1 °C min^{-1} cooling rate is used for all suspensions.

Field-assisted sintering (FAST). The equipment used for sintering is an HPD25 device from FCT System. The linear shrinkage rates were obtained from the movement of the die during the sintering. A constant pressure of 100 MPa was applied during the heat treatment. An electrical field is applied and mainly used to heat the graphite die by the Joule effect. Due to the intensity of the input current, this method provides a high heating rate (around 100 °C min^{-1}). Whether or not the current goes through the sample is not completely clarified yet.

Microstructural characterization. SEM pictures were taken on uncoated samples by a Supra 55 microscope (Zeiss) and a ZEISS NVision40.

Preparation of SENB and bending samples. Beam shaped specimens where cut from the sintered disks and mirror polished. SENB test specimens were first notched with a diamond saw of 200 μm thickness and then the bottom of each notch was sharpened by repeatedly passing a razor blade with diamond paste.

Hardness measurement. We used a MicroMet 6030 microdurometer to measure the hardness on mirror polished samples. The load applied was 0.3 kgf.

Determination of crack length. We used an equivalence between compliance and crack length on an SENB test. The crack length measured is thus the projection of the real crack length at the position of the notch. Sample deflection was measured by a linear variable differential transformer (LVDT) with micrometre accuracy. According to the ASTM criterion[36], the maximum crack extension is given by $\Delta a_{max} = 0.25b$ (b being the uncracked ligament width), which corresponds in our results to $\Delta a = 0.4$ mm.

Details on J-integral calculation. To assess the different mechanisms that occurred during the stable crack propagation, a J-integral versus crack extension has been calculated as the sum of elastic and plastic contributions, a method already used to measure the properties of bone[3,38] and similar structures[12,37]. Full Methods are available in the Supplementary Information.

Received 29 October 2013; accepted 14 February 2014; published online 23 March 2014; corrected after print 10 November 2017

References

1. Ashby, M. F. *Materials Selection in Mechanical Design* 624 (ASTM International, 2010).
2. Ritchie, R. O. The conflicts between strength and toughness. *Nature Mater.* **10,** 817–822 (2011).
3. Koester, K. J., Ager, J. W. & Ritchie, R. O. The true toughness of human cortical bone measured with realistically short cracks. *Nature Mater.* **7,** 672–677 (2008).
4. Peterlik, H., Roschger, P., Klaushofer, K. & Fratzl, P. From brittle to ductile fracture of bone. *Nature Mater.* **5,** 52–55 (2006).
5. Barthelat, F. & Rabiei, R. Toughness amplification in natural composites. *J. Mech. Phys. Solids* **59,** 829–840 (2011).
6. Barthelat, F. *et al.* On the mechanics of mother-of-pearl: A key feature in the material hierarchical structure. *J. Mech. Phys. Solids* **55,** 306–337 (2007).
7. Okumura, K. & De Gennes, P. G. Why is nacre strong? Elastic theory and fracture mechanics for biocomposites with stratified structures. *Eur. Phys. J. E* **4,** 121–127 (2001).
8. Song, F., Soh, A. K. & Bai, Y. L. Structural and mechanical properties of the organic matrix layers of nacre. *Biomaterials* **24,** 3623–3631 (2003).
9. Meyers, M. A., McKittrick, J. & Chen, P-Y. Structural biological materials: Critical mechanics-materials connections. *Science* **339,** 773–779 (2013).
10. Bonderer, L. J., Studart, A. R. & Gauckler, L. J. Bioinspired design and assembly of platelet reinforced polymer films. *Science* **319,** 1069–1073 (2008).
11. Clegg, W. J., Kendall, K., Alford, N. M., Button, T. W. & Birchall, J. D. A simple way to make tough ceramics. *Nature* **347,** 455–457 (1990).
12. Munch, E. *et al.* Tough, bio-inspired hybrid materials. *Science* **322,** 1516–1520 (2008).
13. Erb, R. M., Libanori, R., Rothfuchs, N. & Studart, A. R. Composites reinforced in three dimensions by using low magnetic fields. *Science* **335,** 199–204 (2012).
14. Deville, S. *et al.* Metastable and unstable cellular solidification of colloidal suspensions. *Nature Mater.* **8,** 966–972 (2009).
15. Hunger, P. M., Donius, A. E. & Wegst, U. G. K. Platelets self-assemble into porous nacre during freeze casting. *J. Mech. Behav. Biomed. Mater.* **19,** 87–93 (2013).
16. Herring, C. Effect of change of scale on sintering phenomena. *J. Appl. Phys.* **21,** 301–303 (1950).
17. Zaitsev, A., Litvina, A. D., Mogutnov, B. M. & Tsaplin, A. A. Thermodynamic properties and phase equilibria in the system $CaO\text{-}SiO_2\text{-}Al_2O_3$. *High Temp. Mater. Sci.* **34,** 223–231 (1995).
18. Faber, K. T. & Evans, A. G. Crack deflection processes-I Theory. *Acta Metall.* **31,** 564–576 (1983).
19. Kolednik, O., Predan, J., Fischer, F. D. & Fratzl, P. Bioinspired design criteria for damage-resistant materials with periodically varying microstructure. *Adv. Funct. Mater.* **21,** 3634–3641 (2011).
20. Koester, K. J., Ager, J. W. & Ritchie, R. O. The effect of aging on crack-growth resistance and toughening mechanisms in human dentin. *Biomaterials* **29,** 1318–1328 (2008).
21. Cook, J., Gordon, J. E., Evans, C. C. & Marsh, D. M. A mechanism for the control of crack propagation in all-brittle systems. *Proc. R. Soc. A* **282,** 508–520 (1964).
22. Dimas, L. S. & Buehler, M. J. Tough and stiff composites with simple building blocks. *J. Mater. Res.* **28,** 1295–1303 (2013).
23. Launey, M. E. *et al.* A novel biomimetic approach to the design of high-performance ceramic-metal composites. *J. R. Soc. Inter.* **7,** 741–753 (2010).
24. Munro, R. G. Evaluated material properties for a sintered alpha-alumina. *J. Am. Ceram. Soc.* **28,** 1919–1928 (1997).
25. Pavlacka, R., Bermejo, R., Chang, Y., Green, D. J. & Messing, G. L. Fracture behavior of layered alumina microstructural composites with highly textured layers. *J. Am. Ceram. Soc.* **9,** 1577–1585 (2013).
26. Zhan, G-D., Kuntz, J. D., Wan, J. & Mukherjee, A. K. Single-wall carbon nanotubes as attractive toughening agents in alumina-based nanocomposites. *Nature Mater.* **2,** 38–42 (2003).
27. Tuan, W. H., Wu, H. H. & Yang, T. J. The preparation of Al_2O_3/Ni composites by a powder coating technique. *J. Mater. Sci.* **30,** 855–859 (1995).
28. Travitzky, N., Gutmanas, E. & Claussen, N. Mechanical properties of composites fabricated by pressureless infiltration technique. *Mater. Lett.* **33,** 47–50 (1997).
29. Prielipp, H. *et al.* Strength and fracture toughness of aluminum/alumina composites with interpenetrating networks. *Mater. Sci. Eng. A* **197,** 19–30 (1995).
30. Aghajanian, M. K., MacMillan, N. H., Kennedy, C. R., Luszcz, S. J. & Roy, R. Properties and microstructures of Lanxide Al_2O_3-Al ceramic composite materials. *J. Mater. Sci.* **24,** 658–670 (1989).

31. Chen, R., Chiu, Y. & Tuan, W. Toughening alumina with both nickel and zirconia inclusions. *J. Eur. Ceram. Soc.* **20,** 1901–1906 (2000).
32. Wei, T. *et al.* The effect of carbon nanotubes microstructures on reinforcing properties of SWNTs/alumina composite. *Mater. Res. Bull.* **43,** 2806–2809 (2008).
33. Peigney, A., Laurent, C., Flahaut, E. & Rousset, a. Carbon nanotubes in novel ceramic matrix nanocomposites. *Ceram. Int.* **26,** 677–683 (2000).
34. Yamamoto, G., Omori, M., Hashida, T. & Kimura, H. A novel structure for carbon nanotube reinforced alumina composites with improved mechanical properties. *Nanotechnology* **19,** 315708 (2008).
35. Liu, J., Yan, H. & Jiang, K. Mechanical properties of graphene platelet-reinforced alumina ceramic composites. *Ceram. Int.* **39,** 6215–6221 (2013).
36. ASTM E1820-06, *Annual Book of ASTM Standards, Vol 0301: Metals—Mechanical Testing; Elevated and Low-Temperature Tests; Metallography* (ASTM International, 2006).
37. Launey, M. E. *et al.* Designing highly toughened hybrid composites through nature-inspired hierarchical complexity. *Acta Mater.* **57,** 2919–2932 (2009).
38. Nalla, R. K., Stölken, J. S., Kinney, J. H. & Ritchie, R. O. Fracture in human cortical bone: Local fracture criteria and toughening mechanisms. *J. Biomech.* **38,** 1517–1525 (2005).
39. National Institute of Standards and Technology. NIST Structural Ceramics Database (SCD) (2002); www.ceramics.nist.gov/srd/scd
40. Libanori, R., Erb, R. M. & Studart, A. R. Mechanics of platelet-reinforced composites assembled using mechanical and magnetic stimuli. *ACS Appl. Mater. Interf.* **5,** 10794–10805 (2013).
41. Becher, P. F. Microstructural design of toughened ceramics. *J. Am. Ceram. Soc.* **74,** 255–269 (1991).
42. Rahaman, M. N., Yao, A., Bal, B. S., Garino, J. P. & Ries, M. D. Ceramics for prosthetic hip and knee joint replacement. *J. Am. Ceram. Soc.* **90,** 1965–1988 (2007).
43. Wegst, U. G. K. & Ashby, M. F. The mechanical efficiency of natural materials. *Phil. Mag.* **84,** 2167–2186 (2004).

Acknowledgements

We acknowledge the financial support of the ANRT (Association Nationale Recherche Technologie) and Saint-Gobain through a CIFRE fellowship, convention #808/2010. We are indebted to the Centre Lyonnais de Microscopie (CLYM) for access to the FIB microscope. Acknowledgements are due to Guillaume Bonnefont from MATEIS for his assistance on the sintering equipment, and C. Barentin from the ILM for tipping us on the Carbopol to obtain a yield stress suspension.

Author contributions

S.D. and E.M. designed the research, F.B. processed the sample and performed the mechanical testing, F.B. and S.M. performed the high-temperature mechanical testing, F.B. and B.V.d.M. investigated the structure, all authors analysed and discussed the results, F.B., A.J.S. and S.D. wrote the paper.

Additional information

Supplementary information is available in the online version of the paper. Reprints and permissions information is available online at www.nature.com/reprints. Correspondence and requests for materials should be addressed to S.D.

Competing financial interests

The authors declare no competing financial interests.

Corrigendum: Strong, tough and stiff bioinspired ceramics from brittle constituents

Florian Bouville, Eric Maire, Sylvain Meille, Bertrand Van de Moortèle, Adam J. Stevenson and Sylvain Deville

Nature Materials **13,** 508–514 (2014); published online 23 March 2014; corrected after print 10 November 2017

In the original version of this Article, the R-curves, which quantify how the toughness increases when the crack propagates, were measured following published guidelines (M. E. Launey, *Acta Mater.* **57,** 2919–2932; 2009). Robert Ritchie (Lawrence Berkeley National Laboratory) proposes that the 2013 ASTM E1820 standard (*Standard Test Method for the Measurement of Fracture Toughness*) is a more appropriate guideline. The authors agree, and have therefore corrected the toughness values in the Article to meet the ASTM standard. Specifically, Figs 3c,j and 4 have been amended (shown below), and the original toughness values (in MPa $m^{1/2}$) of 22 (abstract and page 510) and 21 (page 511) have been replaced with 17.3 and 16.4, respectively.

For consistency, the following changes have been made. On page 510, the text "By taking into account the local deflection as well as the other dissipation mechanisms with a J-integral, and by using the equivalence in the stress intensity factor, we find that the maximum increase of toughness is extremely high, around 22 MPa $m^{1/2}$. This corresponds to a 350% increase compared to the K_{Ic} toughness (600% increase with respect to the reference alumina)." has been changed to "According to the ASTM criterion, the maximum increase of toughness is extremely high, around 17.3 MPa $m^{1/2}$. This corresponds to a 300% increase compared to the K_{Ic} toughness (500% increase with respect to the reference alumina)."

On page 512, the sentence "The unique combination of specific strength (σ_f/ρ) and specific toughness (K_c/ρ) of our bioinspired ceramic material actually matches that of engineering aluminium and magnesium alloys (Fig. 4b) while exhibiting higher hardness (16 GPa), stiffness and operating temperature." has been changed to "The unique combination of specific strength (σ_f/ρ) and specific toughness (K_c/ρ) of our bioinspired ceramic material actually matches that of glass-fibre-reinforced plastics (GFRP; Fig. 4b) while exhibiting high hardness (16 GPa), stiffness and operating temperature."

On page 513, the following sentence has been removed: "However, toughness measurements can be considered valid until the data becomes geometry dependent due to large-scale bridging[37], which here corresponds to $\Delta a = 0.8$ mm. The values reported here were thus always obtained within a valid range of crack extension."

In the caption of Fig. 4, "The nacre-like aluminas have specific strength/toughness properties similar to those of titanium or magnesium metallic alloys" has been changed to "The nacre-like aluminas have specific strength/toughness properties similar to those of GFRP".

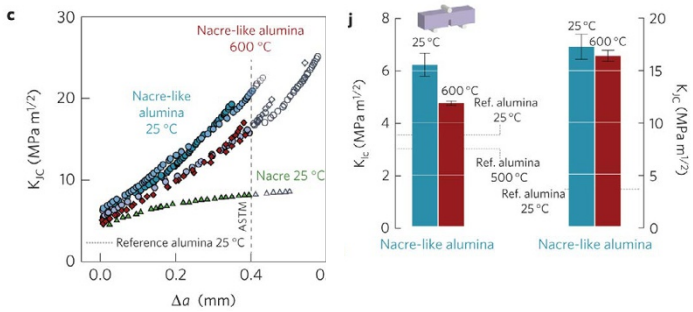

Figure 3

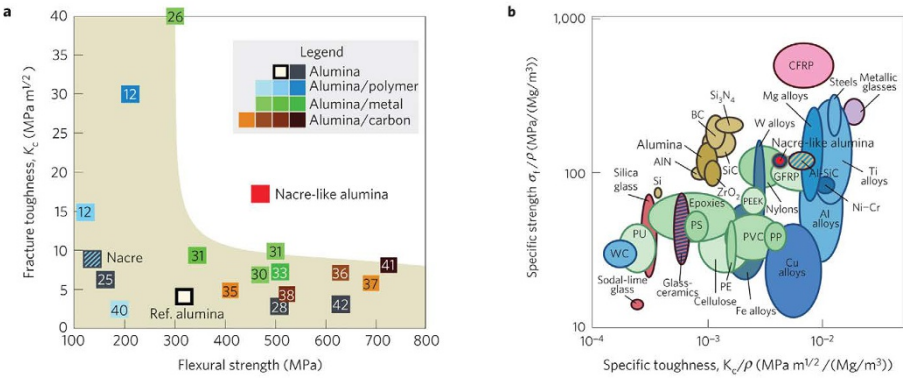

Figure 4